16th World Conference on Earthquake, 16WCEE 2017

Santiago Chile, January 9th to 13th 2017

Paper N° 711 (Abstract ID)

Registration Code: S-D1463117665

NUMERICAL SIMULATION OF UNDERGROUND STRUCTURE BEHAVIORS USING E-DEFENSE LARGE SHAKING TABLE

K. Kaneda[1], Y. Shigeno[1], T. Suzuki[1], S. Nakamura[1], T. Shigeno[1], T. Tojo[1],
N. Nakamura[2], Y. Kawamata[3]

[1] *Chief Researcher, Takenaka corporation,kaneda.kazuhiro@takenaka.co.jp*
[2] *Professor, Hiroshima University, naohiro3@hiroshima-u.ac.jp*
[3] *Researcher, National Research Institute for Earth Science and Disaster Resilience, kawamata@bosai.go.jp*

Abstract

Underground structures connected to each other are often owned by different organizations, designed under different building codes, and constructed in different periods. These differences increase the likelihood that the joints between the structures collapse during a large earthquake. In contrast, underground structures constructed without such differences usually have high seismic performance. In the National Research Institute for Earth Science and Disaster Resilience, large shaking table tests were performed using E-Defense, which is currently the world's largest earthquake simulator, in order to investigate the behavior of underground structures; numerical competitions were planned at that time. In this manuscript, we report on comparisons of experimental results with numerical simulations conducted using three-dimensional finite element method (3D FEM) analyses.

Keywords: Large shaking table, Numerical simulation, Underground structure

1. Introduction

Numerous underground structures, such as subways, vehicle traffic transport tunnels, water supply piping, and ventilation shafts, exist in big cities, and the development of the underground space is proceeding apace all over the world. In Japan, advanced traffic infrastructure involving widespread railway systems constructed deep underground has been discussed. In general, while underground structures are considered to be less susceptible to earthquake damage, the relationship between underground structure and ground deformation and the behavioral particulars resulting from stiffness changes have not been sufficiently clarified.

Japan is well known for its susceptibility to major earthquakes. Recent disasters include the 1995 Hyogoken Nanbu Earthquake, which was a strong local earthquake, and the 2011 Great East Pacific Earthquake, which was a strong inter plate event. In an effort to obtain background information on the results of such events, large shaking table experiments were performed at the National Research Institute for Earth Science and Disaster Resilience in 2012, and a number of technical papers were published based on those results.

In this study, we focused on underground shafts and tunnels in an effort to gain further understanding of the complicated behavior exhibited by underground structures. This paper discusses three-dimensional finite element method (3D FEM) analyses performed on a specimen and compared to the shaking table test results. The analytical simulations were performed before carrying out the experimental test, assuming some initial soil and boundary conditions.

2. Outline of experiment

2.1 Test setup

Figure 1 shows the setup of a test specimen built in a laminar container with an inside diameter of 8 m and a height of 6.5 m. The container is composed of 40 shear rings and two-dimensional (2D) linear sliders positioned between the rings. The specimen was fabricated with two soil strata layers (inclined bedrock and wet sand surface), two vertical shafts interconnected via a cut-and-cover tunnel, and two shield tunnels that crossed the boundary between the bedrock and surface layers.

In order to observe the effectiveness of the flexible portions that are normally used to reduce section stress, 50 mm thick rubber segments were placed at one of the structural joints between the vertical shafts and the cut-and-cover tunnel, as well as along one of the shield tunnels around the soil boundary (Figure 1). The soil and the structure model specifications are summarized in Table 1.

Figure 2 shows the fixity at the bottom of the shafts. Note that movement of aluminum plate welded at the shaft bottoms was fully suppressed by emplacing steel plates arranged in a double cross and then bolting those plates to the bottom of the container. Sufficient fixity could be expected because of the additional resistance provided by embedding the shaft bottoms in cement-mixed sand approximately 1 m thick. Further details of the shaft construction are described in Kawamata et al. (2012).

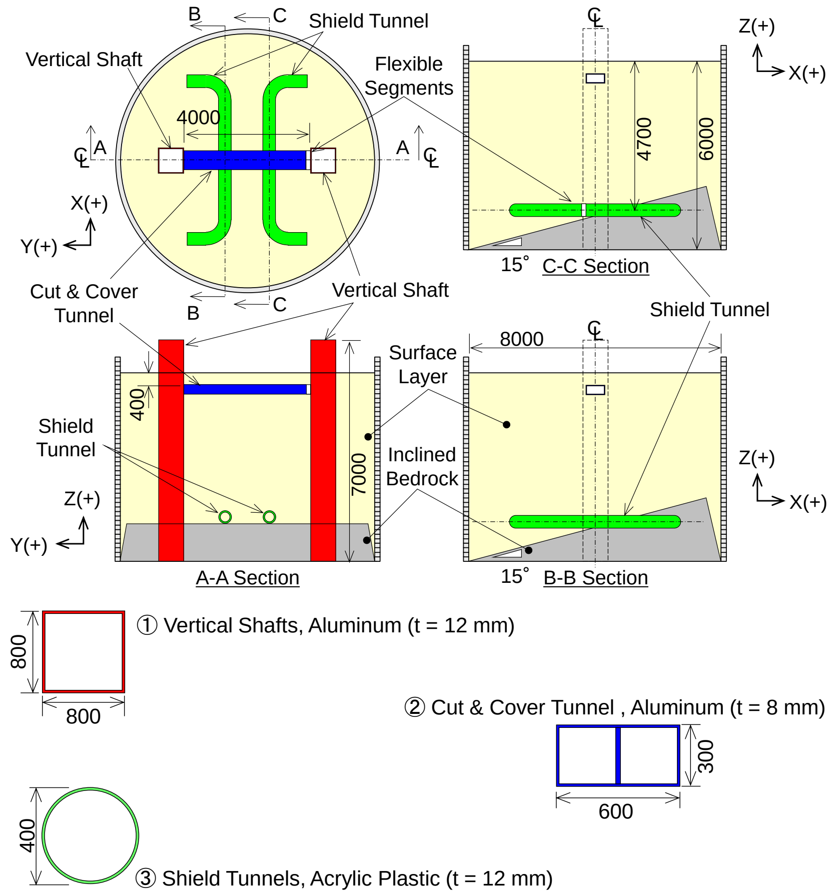

Fig. 1 – Test setup (after Kawamata et al.)

Table 1 – Summary of specifications for soil and structure models

Soil Strata	Material	Unit Weight (kN/m^3)	S-Wave Velocity (m/s)
Surface Layer	Albany Sand		
Bedrock	Cement-mixed Sand		
Structure Models	Material	Outside Dimensions (mm)	Wall Thickness (mm)
Vertical Shafts	Aluminium	800 × 800	12
Cut-and-Cover Tunnel	Aluminium	300(H) × W600(W)	8
Shield Tunnels	Acryl Plastic	ϕ400	8

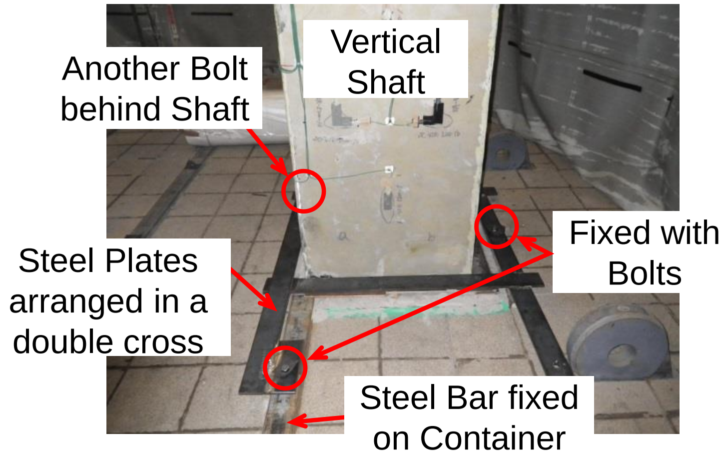

Fig. 2 – Fixity at the bottom of the shafts

2.2 Input motions

Table 2 shows the two input motion types, step sine motions with frequency components of 1 through 20 Hz used as the basic input motion, and 50% and 80% JR Takatori motion (Nakamura et al. 1996), which were applied to the test specimen for this series of shaking table test experiments. Takatori motion is one of the most typical inputs for geotechnical shaking table tests because it provides large ground displacement. Figure 3 compares the target and observed table motions at the time of JR Takatori motion input. From this figure, it is apparent that the motions show a significant level of agreement. In the sections below, the dynamic behaviors resulting from JR Takatori motion in both experiments and numerical simulations are described.

Table 2 – Input motions

	Motion	Acc.Level[1)]	Direction[2)]
1st Day 02/23	Step Sine 1-20Hz	0.1 m/s^2	0 Deg.
		0.1 m/s^2	90 Deg.
		0.3 m/s^2	0 Deg.
		0.3 m/s^2	90 Deg.
		0.3 m/s^2	30 Deg.
		0.3 m/s^2	45 Deg.
		0.3 m/s^2	135 Deg.
2nd Day 02/24	Step Sine 1-20Hz	0.3 m/s^2	90 Deg.
		0.5 m/s^2	0 Deg.
		0.5 m/s^2	90 Deg.
	Takatori	50%	See Note[3)]
3rd Day 02/28	Step Sine 1-20Hz	0.3 m/s^2	90 Deg.
		0.3 m/s^2	0 Deg.
	Takatori	80%	See Note[3)]

1) "Acc.Level" shows the maximum acceleration for Step Sine motions, and amplification from the actual records for Takatori motion.

2) "Direction" means angle from x-axis; i.e. 0 degree is x-axis and 90 degree is y-axis.

3) EW and NS components of Takatori were put in x- and y- axes, respectively.

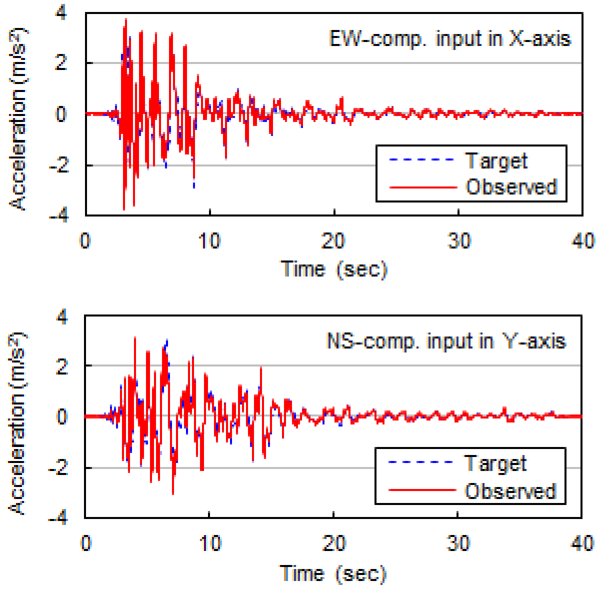

Fig. 3 – Time histories of table motions (Takatori 50%)

3. Simulation Outline

3.1 Simulations model

As previously mentioned, this research focused on 3D FEM analysis-based simulations. In the soil element, the tetrahedral element was set from the bottom to 2250 mm, while the hexahedral element was set from 2250 mm to the top. The cross-sectional form of the shield tunnel was an octagon with a four-node shell element. Fine mesh analyses were conducted near the element between the surface layer and bedrock. The shell was 8 mm thick. A beam element was used at the vertical shaft and cut-and-cover tunnel and was connected with the surrounding soil using a rigid element. A 50 mm clearance was set up at the flexible joint. Four-node shell elements with 100 divisions in the circumference direction and 26 height divisions were set. A 50 mm clearance was also set up at the flexible portion. In total, there were 73,200 elements and 31,321 nodes. Figure 4 shows the numerical meshes. The joint elements between soil and structure were not considered in this study.

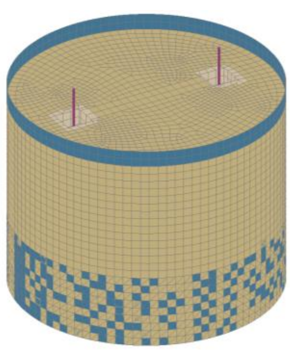

(1) While

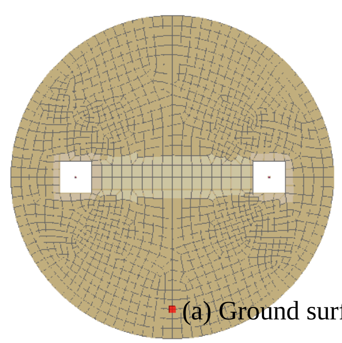

(2) Plane figure

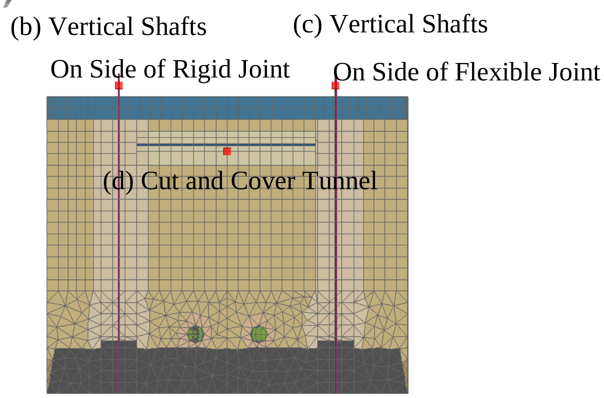

(3) Section figure

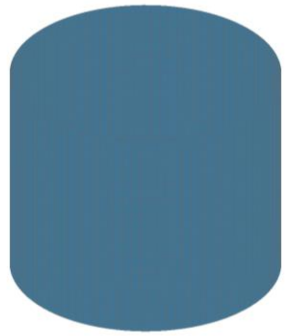

(4) Container

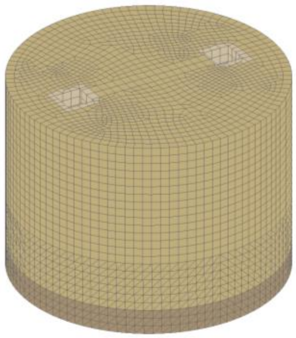

(5) Soil

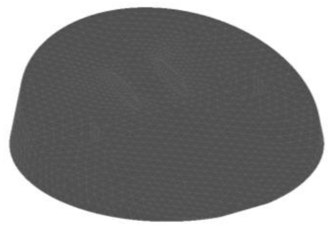

(6) Bedrock

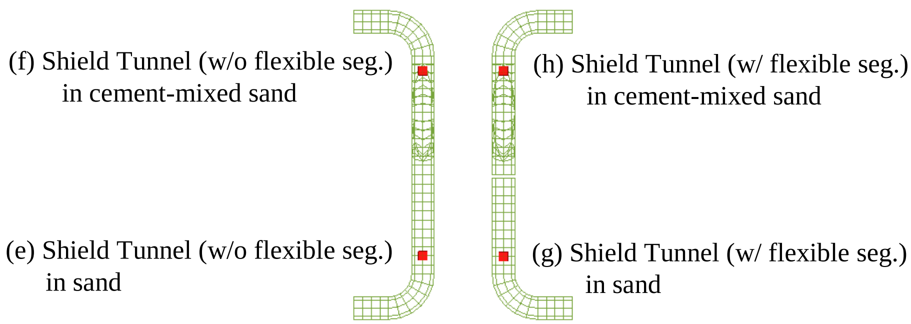

(7) Shield tunnel

(8) Vertical shaft & Cut-and-cover tunnel

Fig. 4 –Numerical mesh

3.2 Soil conditions

In this simulation, a super/subloading yield surface (SYS) modified Cam clay model was used for the soil constituted equation. Using this modified Cam clay model, soil structure behavior was expressed. A superloading surface was introduced to express the soil bulk (structure), an induced anisotropy was introduced to express the soil, and a subloading surface was introduced to express overconsolidation. See Asaoka et.al. (2002) for details. Table 3 shows the soil material constants. We will now explain the method used to determine the soil material constants. Initial shear stiffness G was induced as Eq. 1, which shows the Poisson's ration ν, swelling coefficient κ, void ratio e, and mean effective stress p', respectively. Figure 5 shows the initial measured shear velocity distribution in our experiment.

$$G = \frac{3(1-2\nu)}{2(1+\nu)}\frac{1+e}{\kappa}p' \qquad (1)$$

In general, when the confining pressure increases, shear velocity increases as well. Surface shear velocity was considered to be 100 m/s. Here, the surface confined stress p'=12 kN/m^2 and void ratio e=0.75 were applied in Eq. 1 in order to obtain the initial shear stiffness with soil density 1.6 g/cm^3. Both the measured and simulation shear stiffness are almost same. At first, when the initial shear velocity was given and used, the Poisson ratio and swelling coefficient were determined. Figure 6 shows experimental and simulation results of the undrained triaxial compression test under a confinement pressure of 50 kN/m^2. The initial stiffness valued set for both the experiment and the simulation were found to be unsuitable, most likely due to the effect of a betting error. However, the simulation results for peak and residual strength were almost always in accord with experimental results. Figure 7 shows simulation and experimental results of the dynamic deformation test. As can be seen in the figure, the simulation results closely matched the experimental results. Based on these results, the initial soil parameters (shown in Table 4) were determined. The structure degree and overconsolidation ratio were presumed to be 1.0.

Table 3 – Soil parameters

Elasto-plastic parameter	
Compression index λ	0.025
Swelling index κ	0.0010
Critical state constant M	2.5
NCL intercept N (at p'=98 kPa)	1.735
Poisson's ratio	0.2
Evolution parameters	
Degradation parameter of structure a(b=c=1)	0.8
Degradation parameter of overconsolidated state m	0.3
Evolution parameter b^r	1.0
Limit of rotation m_b	0.1

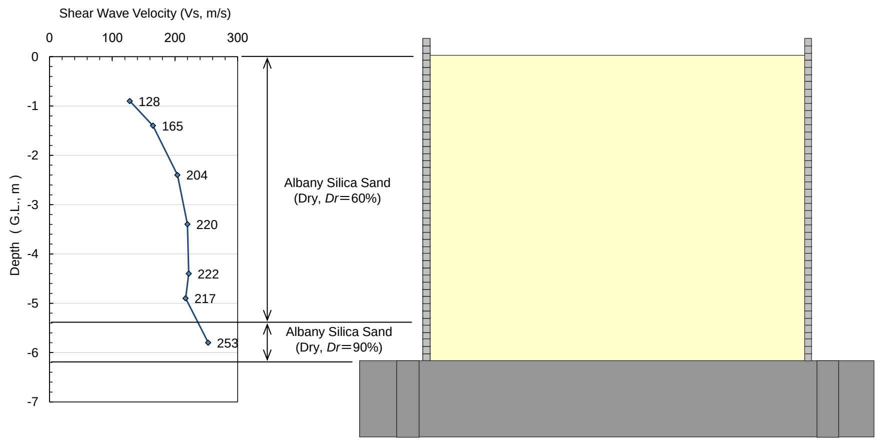

Fig. 5 – Initial measured shear velocity distribution of experiment

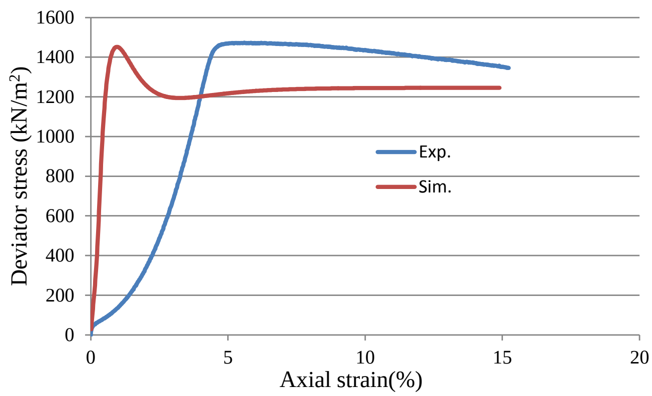

Figure 6 – Undrained triaxial compression test (confining pressure 50 kN/m^2)

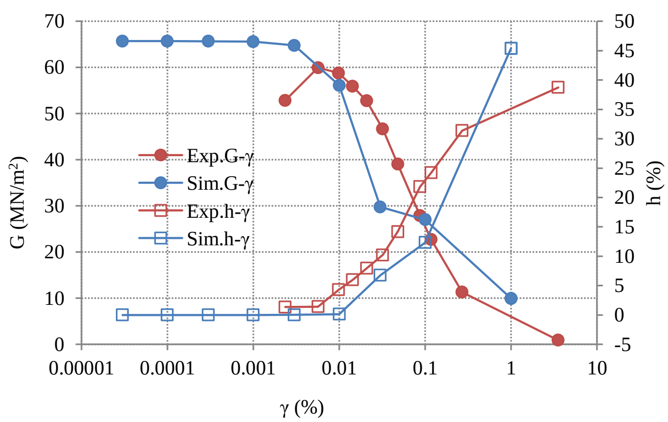

Figure 7 – Dynamic deformation test (confining pressure 50 kN/m^2)

Table 4 – Initial parameters

Coefficient of lateral pressure K_0	0.5
Degree of anisotropy β_0	0. 75
Degree of structure R^*	1.00
Degree of overconsolidation R	1.00

3.3 Structure material

The typical material parameters of structure were shown in Tables 5 to 8. The elastic parameters of structures were set.

Table 5 – Vertical shafts (BAR)

Section : □800×800×t12 MAT : Aluminum

E (kN/m^2)	ν	ρ (t/m^3)	Ax (m^2)	Ay (m^2)	Az (m^2)	Ix (m^4)	Iy (m^4)	Iz (m^4)
6.91E7	0.35	2.7	3.782E-2	1.920E-2	1.920E-2	5.872E-3	3.915E-3	3.915E-3

Table 6 – Cut-and-cover tunnel (BAR)

Section : W600×H300×t8 MAT : Aluminum

E (kN/m2)	ν	ρ (t/m3)	Ax (m2)	Ay (m2)	Az (m2)	Ix (m4)	Iy (m4)	Iz (m4)
6.91E7	0.35	2.7	1.414E-2	9.600E-3	4.800E-3	5.408E-4	2.352E-4	6.862E-4

Table 7 – Shield tunnel (SHELL)

Section : D400×t8 MAT : Acrylic

t (m)	E (kN/m^2)	ν	ρ (t/m^3)
0.008	3.33E6	0.40	1.2

Table 8 – Laminar container (SHELL)

MAT : Rubber

T (m)	E (kN/m^2)	ν	ρ (t/m^3)
0.1	4.00E3	0.48	3.189

3.4 Damping

Rayleigh damping was adopted for both structure and soil damping. Table 9 shows the Rayleigh damping coefficient. As shown in Table 9, Rayleigh damping was considered for both structure and soil. In the structure, α and β were determined by f1=3Hz, f2=10Hz and h=2%.

The simulations were performed using the Takenaka Corp.'s MuDIAN application program on an IBM IDataPlex dx360 M2 server equipped with two Xeon X5570 processors and 48 GB of memory. In our experiment, the step sine wave was loaded first, after which the irregular wave (JR Takatori wave) was loaded. In contrast, only the JR Takatori waves in both X and Y directions were loaded in the numerical simulation.

Table 9 – Coefficient of Rayleigh dumping

	α	β
Soil	0.140100	0.01507
Structure	0.579986	0.00049

4. Comparison between simulation and experiment

Figure 4 shows the measurement point of the simulation shown at the red point. In this paper only acceleration time histories are shown. Figure 8 (a) to (h) show the ground surface, vertical shaft top on the rigid joint side, vertical shaft top on the flexible joint side, cut-and-cover tunnel, shield tunnel (w/o flexible seg.) in sand, shield tunnel (w/o flexible seg.) in concrete-mixed sand, shield tunnel (w/ flexible seg.) in sand, and shield tunnel (w/ flexible seg.) in concrete-mixed sand, respectively. Both simulation and experimental results are shown. Table 10 shows the maximum and minimum acceleration levels.

In the case of (a), it can be seen that the simulation results of the X direction acceleration time history nearly matched the experimental data. However, the simulation results of the Y direction acceleration time history were smaller than the experimental results, apparently due to the soil stiffness effect. In the case of (b) and (c), while simulation and experiment showed similar tendencies, the simulation results of the maximum or minimum acceleration were smaller than the experimental results, apparently due to the structure effect. This indicates that damping or soil deformation is affected as well. In the case of (d), the X direction simulation results of the maximum or minimum acceleration were larger than those obtained via experiment, and the Y direction results showed opposite tendencies, possibly due to the effect of the vertical shaft connection. In the cases of (e) to (h), the simulation results closely matched the experimental results, primarily due to the linear area near the bedrock.

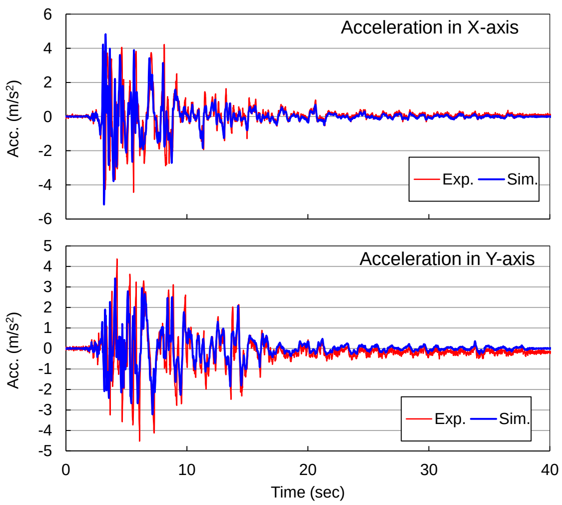

(a) Ground surface

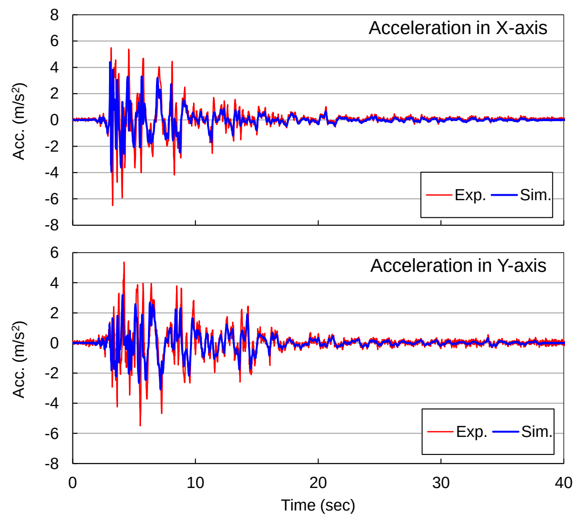

(b) Top of Vertical Shaft on Rigid Joint Side

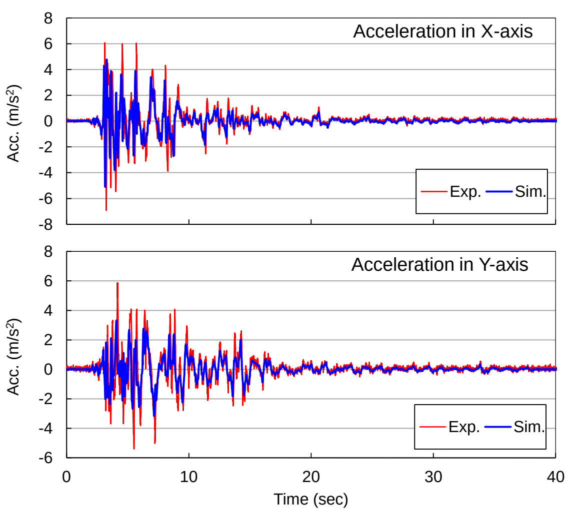

(c) Top of Vertical Shaft on Flexible Joint Side

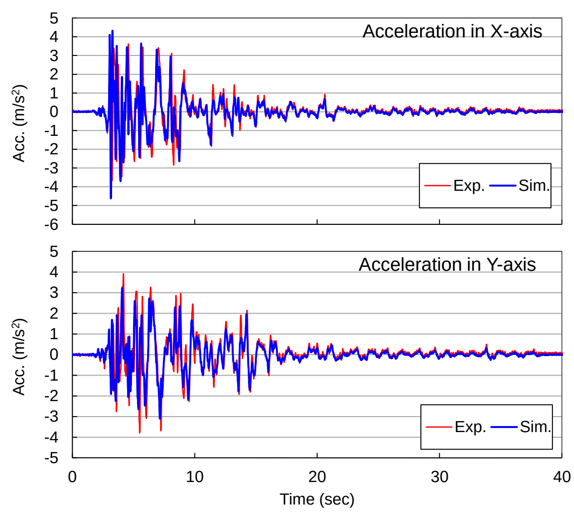

(d) Cut-and-Cover Tunnel

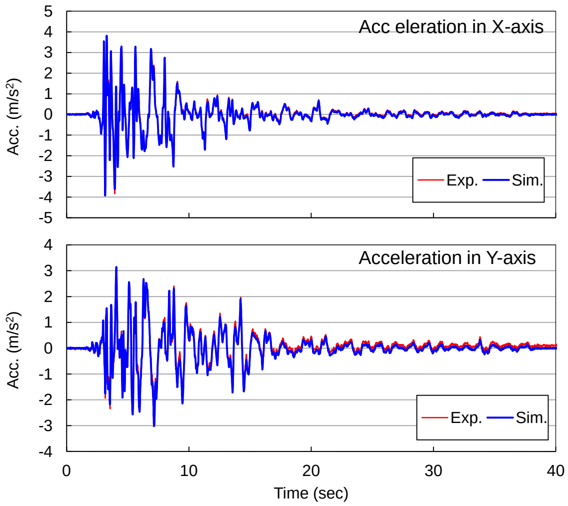

(e) Shield Tunnel (w/o flexible seg.) in Sand

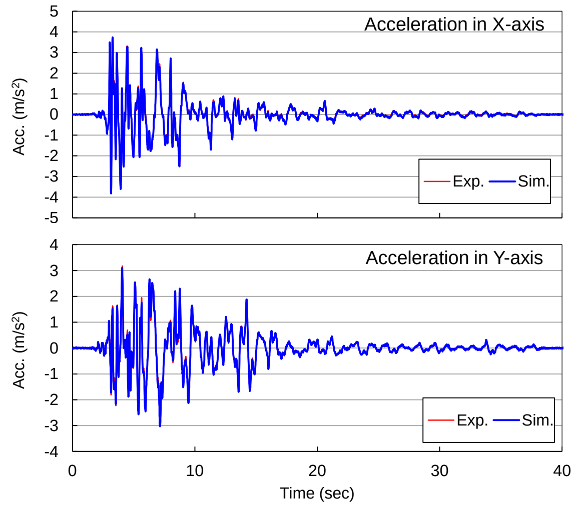

(f) Shield Tunnel (w/o flexible seg.) in C-mixed Sand

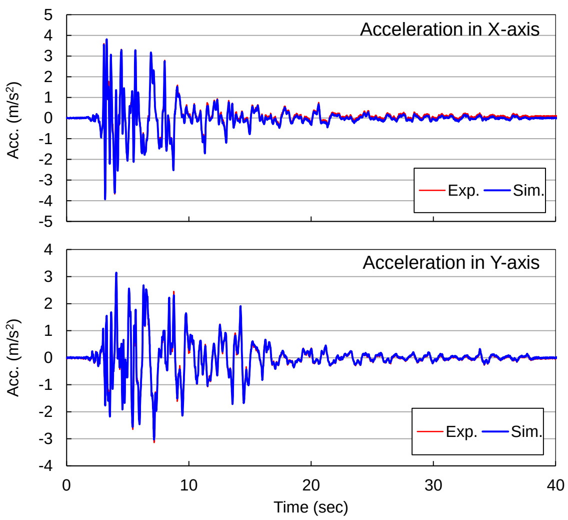

(g) Shield Tunnel (w/ flexible seg.) in Sand

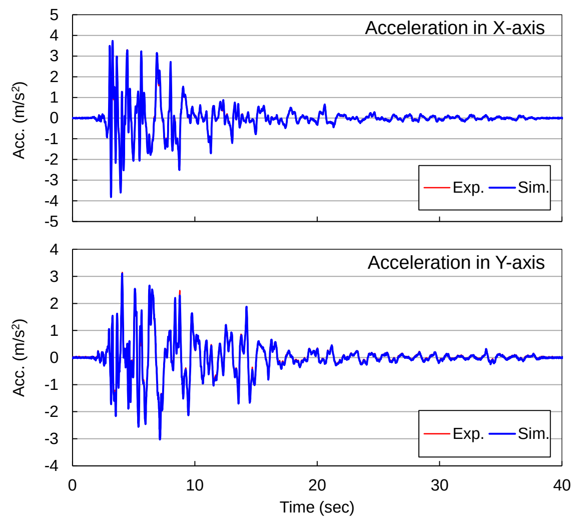

(h) Shield Tunnel (w/ flexible seg.) in C-mixed Sand

Figure 8 – Time history comparison between simulation and experiment

Table 10 – Comparison of maximum and minimum accelerations

		Max(m/s^2)		Min(m/s^2)	
		Exp.	Sim.	Exp.	Sim.
(a)	Ground surface x	4.22	4.83	-4.44	-5.16
	Ground surface y	4.36	3.42	-4.52	-3.22
(b)	Top of Vertical Shaft on Rigid Joint Side X	5.50	4.41	-6.51	-3.94
	Top of Vertical Shaft on Rigid Joint Side Y	5.37	3.18	-5.50	-3.08
(c)	op of Vertical Shaft on Flexible Joint Side X	6.07	4.79	-6.92	-5.10
	op of Vertical Shaft on Flexible Joint Side Y	5.87	3.30	-5.40	-3.16
(d)	Cut-and-Cover Tunnel X	3.62	4.33	-3.67	-4.62
	Cut-and-Cover Tunnel Y	3.92	3.24	-3.80	-3.10
(e)	Shield Tunnel (w/o flexible seg.) in Sand X	3.42	3.81	-3.84	-3.93
	Shield Tunnel (w/o flexible seg.) in Sand Y	3.09	3.14	-2.88	-3.03
(f)	Shield Tunnel (w/o flexible seg.) in C-mixed Sand X	3.44	3.74	-3.62	-3.82
	Shield Tunnel (w/o flexible seg.) in C-mixed Sand Y	3.18	3.11	-2.77	-3.03
(g)	Shield Tunnel (w/ flexible seg.) in Sand X	3.61	3.81	-3.68	-3.93
	Shield Tunnel (w/ flexible seg.) in Sand Y	2.82	3.15	-3.14	-3.02
(h)	Shield Tunnel (w/ flexible seg.) in C-mixed Sand X	3.57	3.74	-3.59	-3.82
	Shield Tunnel (w/ flexible seg.) in C-mixed Sand Y	3.15	3.11	-2.90	-3.03

5. Remarks

Large shaking table tests that had been performed on the E-Defense earthquake simulator were numerically simulated via 3D FEM analyses performed using the initially given soil and structure conditions. Our comparisons showed that the acceleration time history simulation nearly matched the experimental results. However, there was less agreement in the surface, joint side, and rigid side acceleration time histories. It is believed that a reconsideration of the soil parameters will be needed to improve the analysis accuracy, and that it will be necessary to consider structure effects when a larger acceleration value is used.

6. References

[1] Ohtani, K., Ogawa, N., Katayama, T. and Shibata, H. (2003) "Construction of E-Defense (3-D full-scale earthquake testing facility)", 2nd International Symposium on New Technologies for Urban Safety of Mega Cities in Asia, pp. 69-76.

[2] Kawamata, Y., Nakayama, M., Towhata, I., Yasuda, S. and Tabata, K. (2012) "Large-scale Experiment using E-Defense on Dynamic Behaviors of Underground Structures during Strong Ground Motions in Urban Areas", Proceedings of the 15th world conference of earthquake engineering. Lisbon, Portugal.

[3] Kawamata, Y., Nakayama, M., Towhata, I. and Yasuda, S. (2016) "Dynamic behaviors of underground structures in E-Defense shaking experiments", Soil Dynamic and Earthquake Engineering, Vol.82, pp. 24-39.

[4] Asaoka, A., Noda, T., Yamada, E., Kaneda, K. and Nakano, M. (2002)"An elasto-plastic description of two distinct volume change mechanisms of soils", Soils and Foundations, Vol.42, No.5, pp. 47-57.

[5] Shiomi, T., Shigeno, Y. and Zienkiewicz, O.C. (1993) "Numerical prediction for model No. 1, Verification of Numerical Procedures for the Analysis of Soil Liquefaction Problems (eds. By Arulanandan and Scott)", Balkema, pp. 213-219.

[6] Nakamura, Y., Uehan, F. and Inoue, H. (1996) "Waveform and its Analysis of the 1995 Hyogo-Ken-Nanbu Earthquake (II)", JR Earthquake Information No. 23d.